American Mineralogist, Volume 91, pages 285–294, 2006

Hydrogen incorporation in olivine from 2–12 GPa

JED L. MOSENFELDER,* NATALIA I. DELIGNE, PAUL D. ASIMOW, AND GEORGE R. ROSSMAN

Division of Geological and Planetary Sciences, California Institute of Technology, M/C 170-25, Pasadena, California 91125-2500, U.S.A.

ABSTRACT

We performed new experiments on incorporation of hydrogen in olivine at high pressures (2–12 GPa) and temperatures (1000–1300 °C). OH concentrations were calculated using the Bell et al. (2003) calibration applied to principal-axis infrared absorption spectra synthesized from polarized measurements on randomly oriented grains. Starting materials for the experiments included both fine-grained powders and larger single crystals. Hydrogen was incorporated during grain growth in the former case and by volume diffusion in the latter. The spectra of Fe-bearing olivines exhibit similar structure regardless of the starting material, and are dominated by bands in the wavenumber range from about 3500 to 3650 cm^{-1}. We do not observe bands at 3525 and 3573 cm^{-1}, which are predominant in many natural olivines as well as olivines annealed in experiments at lower pressures, and are attributed to humite-related defects. Furthermore, bands between 3300 and 3400 cm^{-1}, attributed to high silica activity or high oxygen fugacity, are weak or non-existent. Our measurements indicate that OH solubility in Fe-bearing olivine is 2.5–4 times higher than that measured by Kohlstedt et al. (1996). Although this is largely due to the use of a new calibration in our study, correction of previous values is not straightforward. In the pure Mg-system, in contrast to Fe-bearing olivine, order-of-magnitude apparent differences in OH solubility can be obtained using different experimental procedures. This raises questions about attainment of equilibrium in experimental studies of hydrogen incorporation in nominally anhydrous minerals, particularly when crystals are grown from a hydrous melt.

Keywords: Spectroscopy, infrared, water, mantle

INTRODUCTION

The importance of nominally anhydrous minerals (NAMs) as storage sites for water in the mantle was recognized over thirty years ago by Martin and Donnay (1972). This topic has received increasing attention over the past two decades as a result of new work on natural and synthetic NAMs as well as widespread recognition of the important influence of even trace amounts of OH on geochemical and geophysical processes (e.g., Hirth and Kohlstedt 1996; Asimow and Langmuir 2003; Karato 2003; Dixon et al. 2004). Experimental data suggesting that water storage capacity increases dramatically in the mantle transition zone (Smyth 1994; Kohlstedt et al. 1996; Bolfan-Casanova et al. 2000) has paved the way for an intriguing, though speculative, model to explain the interplay between mantle convection and the geochemical evolution of the Earth (Bercovici and Karato 2003). Seismological and magnetotelluric studies are also providing more evidence for the existence of hydrated zones in the mantle (Karato 2003; Tarits et al. 2004).

Much of the attention on NAMs has been focused on olivine, the predominant mineral of the upper mantle. Pioneering experimental work (Bai and Kohlstedt 1993; Kohlstedt et al. 1996) revealed systematic trends of hydrogen incorporation in Fe-bearing olivine as a function of water and oxygen fugacity, silica activity, and pressure. However, recent developments have raised new questions and controversies. First, Bell et al. (2003) presented a new calibration for H measurement in olivine using Fourier-transform infrared (FTIR) spectroscopy. Their work suggests that previous solubility measurements need to be revised upward by a factor of 2 to 4, but emphasizes that retrospective application of the calibration is complicated by reliance on unpolarized spectra in those studies. Second, experiments by different groups have yielded highly varying estimates for OH solubility in nominally Fe-free forsterite (Kohn 1996; Keppler and Rauch 2000; Locke et al. 2001; Demouchy and Mackwell 2003; Lemaire et al. 2004; Zhao et al. 2004). Third, previous results (Bai and Kohlstedt 1993) with regard to the effect of silica activity on OH speciation have been contradicted by new experimental studies (Matveev et al. 2001; Lemaire et al. 2004). Fourth, another series of experiments suggests that the presence of Ti is critical to incorporation of OH in olivine (Berry et al. 2004). Finally, new data has been brought to bear on the nature of nanometer-scale inclusions of hydrous phases in olivine (Khisina et al. 2001; Khisina and Wirth 2002; Kudoh 2002; Matsyuk and Langer 2004).

In light of these developments, we conducted a new experimental study of hydrogen incorporation in olivine at pressures of 2–12 GPa and temperatures of 1000–1300 °C. In this study, we employ a new technique for FTIR measurement of OH concentrations in olivine that accounts for the correction of polarized spectra on randomly oriented crystals. The full details of this technique are provided in a separate paper (Asimow et al. 2006).

EXPERIMENTAL AND ANALYTICAL METHODS

Details of the experiments, including starting materials, encapsulation, conditions, and final OH concentrations, are summarized in Table 1 and discussed below.

Starting materials

Most of our experiments employed fine (1–10 μm) or coarse (417–495 μm) powders of olivine made by crushing single crystals from Kilbourne Hole (New

* E-mail: jed@gps.caltech.edu

0003-004X/06/0203–285$05.00/DOI: 10.2138/am.2006.1943

Mexico), San Carlos (Arizona), and Zabargad Island (Egypt). The forsterite content of all these olivines lies in the range $Fo_{89.5–90.5}$ (Beran and Putnis 1983; Kohlstedt et al. 1996; Wasylenki et al. 2003). Olivine from the first two localities is almost hydrogen-free (less than 1 ppm H_2O), whereas the Zabargad olivine contains ~5–10 ppm H_2O and has unique IR spectra (Beran and Putnis 1983), indicative of the presence of humite-type defects (Miller et al. 1987). Fine-grained (1–10 μm) orthopyroxene powder was also added to some experiments to influence silica activity. The orthopyroxene, from Kilbourne Hole, has Mg no. [100 × molar Mg/(Mg + Fe)] = 90.7. The full composition is given by Wasylenki et al. (2003).

Hydrogen incorporation in nominally pure (Fo_{100}) forsterite was investigated using two different starting materials. The first material was a fine-grained powder synthesized by sintering dried, high-purity MgO and SiO_2 weighed, and mixed together in stoichiometric amounts. The mixed oxides were fired at 1550 °C in a Deltech furnace for 24 h, followed by crushing, mixing, and firing again under the same conditions. X-ray diffraction of the final powder showed nearly pure forsterite with minor amounts of excess MgO. For experiment ww331, we used two oriented forsterite crystals cut from a single crystal synthesized by H. Takei using the Czochralski method (Takei and Kobayashi 1974). These crystals are from the same boule used by Zhao et al. (2004). The dimensions of the crystals were 400 μm (along the *a*- and *c*-axes) by 600 μm (along the b-axis). Measured impurities include Fe (several hundred ppm) and <20 ppm of Ir, Na, and Ca (see Takei and Kobayashi 1974 and Zhao et al. 2004 for details). The crystals were placed within the capsule such that the b-axis of one crystal and the c-axis of the other were vertically aligned with respect to the press.

Water in most of the experiments was produced by dehydration under the run conditions of a 1.4:1 (by weight) mixture of synthetic talc and brucite (cf. Kohlstedt et al. 1996). The amount of this mixture used in each experiment was chosen so as to provide a nominal total concentration of 1–3 wt% H_2O. For experiments with fine-grained olivine, the talc and brucite were intimately mixed with the olivine. In the other experiments, the mixture was packed into the bottom of the capsule below the layer of orthopyroxene. The two experiments conducted on nominally pure forsterite employed only brucite as a water source.

High-pressure experiments

A 1000-ton press and Walker-type multi-anvil module were employed for experiments at 5–12 GPa and 1000–1300 °C. The experimental durations were chosen so as to ensure grain growth (Karato 1989) in runs where fine-grained olivine was used, and to ensure equilibration in experiments using larger crystals, based on the diffusion data of Kohlstedt and Mackwell (1998). Truncated Toshiba "F" grade WC cubes (32 mm edge-length) were used as second-stage anvils to compress octahedral 14/8 (octahedral edge length (OEL)/cube truncation edge length (TEL) in mm) and 18/11 pressure assemblies. The assemblies were comprised of semi-sintered, Cr-doped MgO octahedra containing zirconia insulating sleeves around stepped furnaces made of either $LaCrO_3$ (14/8) or graphite (18/11). We used pyrophyllite gaskets (4.5 mm wide × 2.8 mm thick for the 14/8, and 5 mm wide × 3.24 mm thick for the 18/11), and paper and Teflon tape behind the gaskets for support and electrical insulation. The design of the 18/11 is identical to the 18/8 design illustrated in Frost et al. (2004), but without the high-temperature modification. Temperature was controlled in all experiments using axial W_5Re-$W_{26}Re$ thermocouples, with no correction made for the effect of pressure on EMF.

Pressure calibrations for both assemblies are shown in Figure 1. The 14/8 assembly was calibrated at room temperature against the Bi I-II and Bi II-III transitions (Getting 1998) and at 1200 °C by bracketing the following transitions: $CaGeO_3$ garnet-perovskite (Susaki et al. 1985), coesite-stishovite (Zhang et al. 1996), and Mg_2SiO_4 forsterite-wadsleyite (Morishima et al. 1994). The 18/11 assembly was calibrated against the $CaGeO_3$ and coesite-stishovite transitions at 1200 °C. All calibration experiments at high temperature employed a mixture of both low-pressure (50 to 80 wt%) and high-pressure (20–50 wt%) phases, previously synthesized in separate experiments. Sample capsules were made of thin Re foil for the 14/8, and of compound $Ni/Au_{75}Pd_{25}$ capsules for the 18/11 (see below). Pressure and temperature uncertainties of multi-anvil experiments are difficult to assess, but are considered to be ±0.5 GPa and ±30 °C, respectively (Rubie 1999).

Initial hydration experiments using welded 1.8 mm O.D. Pt and 1.6 mm O.D. $Au_{75}Pd_{25}$ capsules were mostly unsuccessful in retaining excess H_2O (Table 1). The best retention was achieved by employing a miniaturized version of the compound capsule technique reported by Ayers et al. (1992). These capsules were comprised of an outer Ni jacket (2.4 mm O.D. /1.6 mm I.D.) with a $Au_{75}Pd_{25}$ inner liner (1.6 mm O.D. /1.3 mm I.D.), a 0.3 mm thick $Au_{75}Pd_{25}$ gasket, and a 0.5 mm thick Ni lid. The surfaces of the Ni capsule and lid were oxidized by firing at 1000 °C in air for 12 h. The resulting thin layer of NiO serves to buffer oxygen fugacity during the experiment and to retard Ni diffusion through the noble metal liner into the sample (Ayers et al. 1992). The high thermal conductivity and large volume of the capsule also helps to reduce temperature gradients (Ayers et al. 1992). The capsules

TABLE 1. Experimental conditions and measured OH concentrations

Run no.	Assembly*	*P*†	*T*	f_{H_2O}‡	Duration	Capsule§	Oxygen buffer‖	Starting material (mg)#			H_2O	C_{OH} Bell Calibration	C_{OH} Paterson Calibration**
		GPa	(°C)	GPa	hours			T/B	Ol	Opx	present?	(wt ppm H_2O)	(wt ppm H_2O)
Piston-cylinder													
R056	1.91 cm	2 (1.8)	1300	8.4	48	AuPd	none	9.9	154.4 (fg,KLB)	na	Yes††	375	115/54
Multi-anvil (Fe-bearing)													
ww296	18/11	5.65	1000	2.36×10^3	24	Ni/AuPd	NNO	1	2.7 (cg, SC)	2.0	Yes	2113	705/531
ww329	18/11	6	1000	3.66×10^3	25	Ni/AuPd	NNO	1.2	3.0 (cg,SC)	0.4	Yes	1705	627/461
ww327	18/11	6	1100	2.63×10^3	8	Ni/AuPd	NNO	1.9	2.0 (cg,SC)	0.3		1451	494/362
ww328	18/11	6	1100	2.63×10^3	8	Ni/AuPd	NNO	1.9	1.8 (cg,SC)	0.3		1730	568/454
ww228	14/8	6	1150	2.26×10^3	24	Pt	none	0.5	7.1(fg,KLB)	na		1576	457/360
ww317	18/11	8	1000	4.03×10^4	30	Ni/AuPd	NNO	0.8	3.1 (cg,SC)	0.5	Yes	3032	1033/762
ww320	18/11	8	1100	2.51×10^4	24	Ni/AuPd	NNO	0.9	3.4 (cg,SC)	0.5		3007	950/678
ww322	18/11	8	1100	2.51×10^4	12	Ni/AuPd	NNO	1.2	2.4 (cg,SC)	0.7		3035	997/718
ww323	18/11	8	1100	2.51×10^4	8	Ni/AuPd	NNO	2.1	1.9 (cg,SC)	0.3	Yes	1657	538/440
ww227	14/8	8	1150	2.03×10^4	24	Pt	none	0.5	7.3 (fg,KLB)	na		2177	678/516
ww325	18/11	8	1200	1.66×10^4	4	Ni/AuPd	NNO	2	2.4 (cg,SC)	0.2	Yes	2398	803/626
ww263	14/8	10	1200	1.21×10^5	24	AuPd	none	1.05	5.6 (fg,KLB)	na	Yes	5055	1700/1170
ww268	14/8	10	1200	1.21×10^5	24	AuPd	NNO	0.8	4.5 (fg,KLB)	na		1141	416/322
ww256	14/8	10	1250	9.74×10^4	24	Pt	none	1.1	5.9 (fg,ZB)	na		1895	661/465
ww225	14/8	12	1100	1.48×10^6	24	Pt	none	0.4	5.7 (fg,KLB)	na		6399	2267/1565
Multi-anvil experiments (nominally Fe-free)													
ww276	14/8	5.65	1175	1.41×10^3	15‡‡	Pt	none	1.0‡‡	7.9 (fg,Fo)	na		2040	935/506
ww331	18/11	6	1200	1.96×10^3	3	Ni/AuPd	NNO	2.5§§	2.0 (cubes,Fo)	na		see text	

* Refers to the cell diameter or OEL/TEL for piston-cylinder and multi-anvil experiments, respectively.
† Number in parentheses is corrected pressure for piston-cylinder experiments.
‡ Determined using the equation of state of Pitzer and Sterner (1994), see text.
§ See text for further explanation.
‖ None = no buffer added; NNO = Oxygen fugacity controlled by Ni-NiO buffer.
Numbers indicate weight in mg of material added. T/B = 1.4:1 talc/brucite mix; Ol = olivine; opx = orthopyroxene; fg = fine-grained; cg = coarse grained; cubes = single crystals, see text; KLB =Kilbourne Hole; SC = San Carlos; ZB = Zabargad Island; Fo = synthetic forsterite .
** Numbers calculated from polarized/unpolarized spectra, respectively, see text.
†† "Yes" indicates that excess water was clearly present at the end of the experiment (see text for more information).
‡‡ This experiment was run for 15 hours at 1300 °C and 15 hours at 1175 °C.
§§ Only brucite added.

were insulated from the stepped graphite furnace by a thin MgO sleeve, and the thermocouple was separated from the top of the sample capsule by a 0.3 mm thick disk of fully dense alumina, to prevent thermocouple contamination. Cold-welding of the capsules took place during compression, which typically lasted from 3 to 6 h. All samples were quenched to less than 400 °C within 5–10 seconds by cutting power to the furnace at the completion of each experiment.

We also report the result of a hydration experiment conducted at 2 GPa (nominal pressure) and 1300 °C for 48 h. This was performed in an end-loaded piston-cylinder apparatus using a 1.91 cm CaF_2-graphite pressure assembly. Temperature was controlled using a W_3Re-$W_{26}Re$ thermocouple and held constant to ±2 °C. Preliminary calibrations at 600 and 800 °C against the equilibria albite-jadeite-quartz (Holland 1980) and quartz-coesite (Bohlen and Boettcher 1982) suggest that a negative pressure correction of ~0.2 GPa should be applied to the nominal pressure. The sample for the hydration experiment was contained in a welded 5 mm O.D. $Au_{75}Pd_{25}$ capsule.

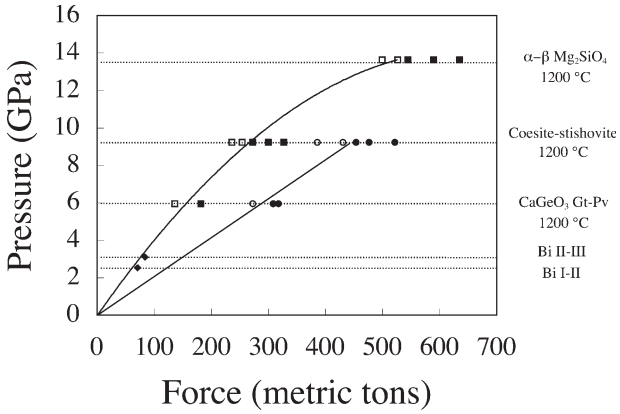

FIGURE 1. Pressure calibration curves for the 14/8 and 18/11 multi-anvil assemblies. Unfilled and filled symbols represent reversal brackets to the low- and high-pressure side of each reaction, respectively. Squares and circles are for 14/8 and 18/11 calibrations, respectively. Filled diamonds represent the location of the Bi I-II and Bi II-III transitions during compression of a 14/8 assembly. The lines are polynomial and linear fits to the midpoints of the brackets for the 14/8 and 18/11 calibrations, respectively.

Following decompression, all samples were pierced to check for excess water, which provides strong evidence for water-saturation in subsolidus experiments. The capsules were then cut in half to prepare polished sections for analysis. For experiment ww331, two thin sections were made to intersect the {010} and {001} planes of the two forsterite crystals. Most capsules were vacuum-impregnated with Petropoxy 151™ to contain friable, loose grains. Sections for FTIR spectroscopy were made using Crystalbond adhesive, which was subsequently dissolved in acetone, followed by cleaning in ethanol and isopropyl alcohol.

FTIR spectroscopy and electron microprobe analysis

Infrared spectra were acquired using a Nicolet Magna 860 FTIR spectrometer coupled to a Spectra-Tech Continuum microscope. Polarized spectra were recorded from 650 to 4000 cm^{-1} by averaging 400 or more scans with 2 cm^{-1} resolution, using a GLOBAR infrared light source, a KBr beamsplitter, a CaF_2 wire-grid polarizer, and an MCT-A detector. We used square, 30 to 200 μm wide apertures to collect spectra from regions as free as possible from cracks and grain boundaries.

For each sample, polarized spectra were collected for multiple, randomly oriented crystals, with the E-vector (**E**) parallel to the two extinction positions of each grain. Because the orientations of the crystals were not known a priori, we developed a new method to use these data to synthesize a consistent set of spectra corresponding to **E**lla, **E**llb, and **E**llc (note we use the same convention for these directions in olivine as Bell et al. 2003). The technique is based on comparison of polarized absorbance spectra between unknowns and standards in the silicate overtone region, from ~1500 to 2200 cm^{-1}. The standards were X-ray oriented slabs of single-crystal San Carlos olivine and synthetic forsterite. Full details of the method, including background corrections and other experimental issues, are given by Asimow et al. (this issue). The orientations of crystals close to zone axes were also verified using Raman spectroscopy (see Arredondo and Rossman 2002 for experimental details) and optical microscopy. OH concentrations were determined by applying the calibration of Bell et al. (2003) to the three synthesized, principal-axis spectra over the wavenumber range 2950–3750 cm^{-1}. For the sake of comparison to previous results, we also calculated concentrations using the Paterson (1982) calibration applied to both the synthetic polarized spectra (in three directions) and theoretical "unpolarized" spectra in the (010) plane calculated by averaging (in transmission) polarized **E**lla and **E**llc spectra (see Libowitzky and Rossman 1996). In the latter case we used an "orientation factor" of 0.33.

Wavelength-dispersive chemical analyses were obtained on selected samples using a JEOL 733 microprobe operating at 15 kV and 25 nA beam current. Stan-

TABLE 2. Representative electron microprobe analyses

	ww276	ww276	ww317 Core	ww317 Rim	ww317 Core*	ww227 Core	ww227 Rim	ww325 Core	ww325 Rim
SiO_2	42.08	42.41	41.30	41.52	41.61	41.62	41.52	41.92	40.77
TiO_2	0.01	0.03	0.00	0.01	0.00	0.01	0.02	0.00	0.00
Al_2O_3	0.01	0.00	0.01	0.00	0.01	0.01	0.14	0.11	0.10
FeO	0.00	0.02	7.17	7.14	5.88	8.11	8.22	4.58	4.92
MnO	0.00	0.00	0.10	0.08	0.07	0.15	0.12	0.06	0.06
MgO	57.80	57.66	50.04	50.12	50.81	48.47	48.29	51.87	46.55
CaO	0.01	0.01	0.00	0.00	0.01	0.00	0.01	0.00	0.00
NiO	0.00	0.01	0.47	0.48	0.95	0.34	0.39	0.67	6.63
Na_2O	0.00	0.00	0.00	0.00	0.00	0.00	0.01	0.00	0.00
K2O	0.01	0.02	0.01	0.02	0.02	0.02	0.03	0.01	0.02
Cr_2O_3	0.01	0.00	0.01	0.03	0.00	0.02	0.00	0.01	0.02
Total	99.93	100.15	99.12	99.40	99.37	98.76	98.75	99.23	99.06
Si	0.988	0.993	1.009	1.011	1.010	1.023	1.021	1.011	1.015
Ti	0.000	0.000	0.000	0.000	0.000	0.000	0.000	0.000	0.000
Al	0.000	0.000	0.000	0.000	0.000	0.000	0.004	0.003	0.003
Fe	0.000	0.000	0.147	0.145	0.119	0.167	0.169	0.092	0.102
Mn	0.000	0.000	0.002	0.002	0.001	0.003	0.003	0.001	0.001
Mg	2.023	2.012	1.823	1.820	1.839	1.776	1.771	1.866	1.728
Ca	0.000	0.000	0.000	0.000	0.000	0.000	0.000	0.000	0.000
Ni	0.000	0.000	0.009	0.009	0.019	0.007	0.008	0.013	0.133
Na	0.000	0.000	0.000	0.000	0.000	0.000	0.000	0.000	0.000
K	0.000	0.000	0.000	0.001	0.001	0.001	0.001	0.000	0.001
Cr	0.000	0.000	0.000	0.001	0.000	0.000	0.000	0.000	0.000
Formula total†	7.012	7.007	6.991	6.989	6.990	6.977	6.977	6.987	6.983
Mg no.	1.000	1.000	0.926	0.926	0.939	0.914	0.913	0.953	0.944

* Olivine grain located at bottom of capsule.
† Cations and formula total calculated on basis of four O atoms.

dards included synthetic forsterite and Ni- and Mn-olivines, rutile, fayalite, albite, microcline, and Cr_2O_3. San Carlos olivine (Fo_{90}) was used as a secondary standard. Data processing followed the CITZAF method (Armstrong 1988).

RESULTS

Hydrogen incorporation in Fe-bearing olivine

In experiments using finely powdered Fe-bearing olivine as the primary starting material, significant grain growth took place, resulting in grains with diameters up to ~300 μm (Fig. 2). This extent of grain growth is consistent with the kinetic data of Karato (1989). Unfortunately, only two of these runs (at 2 GPa and 10 GPa) yielded an apparent excess of fluid after the experiment. This can be attributed to several factors. The amounts of talc and brucite added to these experiments were deliberately chosen so as to yield enough water to saturate the experiment, but not to shift the Mg no. of the olivine by more than one unit. Thus, significantly less water was evolved in these experiments than in those of Kohlstedt et al. (1996), who used similar encapsulation techniques and starting materials, but larger proportions of talc and brucite. Our failure to detect excess fluid in the experiments may simply reflect an inability to detect small amounts of water by the "bubbling" method. Moreover, water loss from the Pt and $Au_{75}Pd_{25}$ capsules can be significant. Recent studies provide evidence not only for rapid hydrogen loss, but for oxygen diffusion through capsules as well (e.g., Truckenbrodt and Johannes 1999). Experiments that did not evolve visible bubbles upon piercing are taken to provide lower limits to the OH solubility in olivine at the run conditions.

Nine experiments were conducted using coarser San Carlos olivine crystals and compound Ni/$Au_{75}Pd_{25}$ capsules. Excess fluid was clearly observed in six of these experiments. Thus, this technique was apparently more successful for retaining water than using noble metal capsules alone. Pre-oxidation of a surface layer on the thick Ni outer capsule ensures effective buffering of oxygen fugacity throughout the experiment (Watson and Cherniak 1997). In contrast, in experiments that employ thin Ni liners, the oxygen buffer might become exhausted as a consequence of reaction with the sample (Kohlstedt et al. 1996). Ni diffusion through the inner capsule in experiments at 1000 °C was minimal, but in long duration experiments at 1100 °C (25 h) and at 1200 °C, Ni diffusion into the sample resulted in the formation of Ni-rich rims on the olivine single crystals (Fig. 2c).

Polarized infrared spectra taken through clear portions of crystals in all these experiments show consistent bands for given orientations. No significant zoning of OH concentrations in the crystals was detected (using 50 μm apertures) in any of the experiments. The expected mechanism of incorporation could be different in the experiments using fine- and coarse-grained materials, because in the former case hydrogen is taken up during grain growth, while in the latter case incorporation proceeds by volume diffusion. Simultaneously, in the experiments with coarse single crystals, Mg-rich olivine forms by reaction of talc and brucite at the bottom of the capsule, and hydrogen incorporation in these new olivine crystals must occur during grain growth. Electron microprobe analyses show that this reaction-product

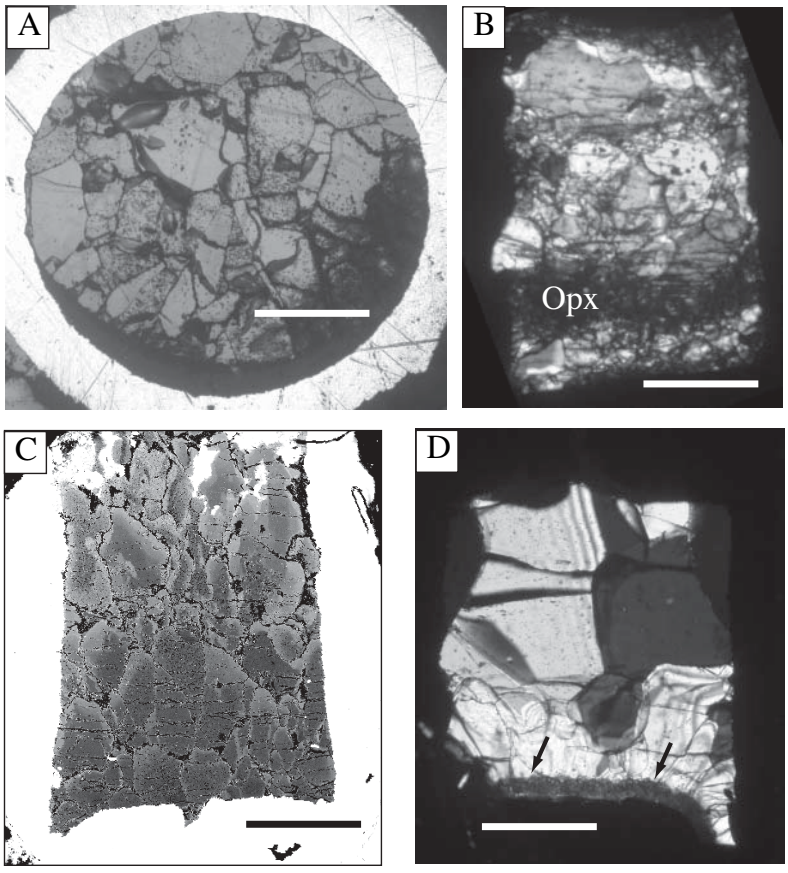

FIGURE 2. Examples of experimental products. All scale bars are 500 μm. (**a**) Experiment ww227 (8 GPa, 1150 °C, 24 h). Olivine grains up to ~300 μm wide grew from a fine-grained powder of Kilbourne Hole olivine mixed with talc and brucite. The dark rind at the bottom of the capsule is the epoxy with which the sample was impregnated. Photograph in reflected light. (**b**) Sample ww317 (8 GPa, 1000 °C, 24 h). San Carlos olivine contained in a Ni/$Au_{75}Pd_{25}$ capsule. The dark band near the bottom of the capsule is a layer of othopyroxene (Opx) added to buffer silica activity. Mg-rich olivine crystals grew from talc and brucite packed into the bottom of the capsule. Photograph in cross-polarized transmitted light. (**c**) Back-scattered electron micrograph of sample ww325 (8 GPa, 1200 °C, 4 h). Ni-rich rims (lighter gray color) formed on olivine crystals as a result of diffusion of Ni through the inner $Au_{75}Pd_{25}$ capsule. (**d**) Large grains of Mg_2SiO_4 forsterite formed from a partial melt (ww276, 5.65 GPa). The experiment was held at 1300 °C for 15 h, and then cooled rapidly to 1175 °C and held for an additional 15 h. Arrows point to a layer of small MgO crystals at the bottom of the capsule. Photograph in cross-polarized transmitted light.

olivine exchanges Mg and Fe with the rest of the charge (Table 2). Despite these fundamentally different processes of hydrogen incorporation and differences in Mg no. of the product olivine, the IR spectra do not significantly differ between the olivine loaded as large starting crystals and the olivine resulting from talc-brucite breakdown.

Figure 3 shows the synthesized spectra from experiment ww227 (at 8 GPa and 1150 °C) corresponding to **E**∥a, **E**∥b, and **E**∥c. The measured spectra that were used to synthesize these principal-axis spectra are shown in Asimow et al. (this issue). This figure also shows spectra from a natural crystal of olivine from Buell Park, Arizona, which contains ~50 ppm H_2O. The comparison reveals a remarkable consistency in band positions and relative peak heights even though the spectra differ by a factor of ~40 in integrated absorption. The spectra from this Buell Park olivine, previously unpublished, are different from the spectra of an orange-brown colored olivine from this locality, which contains planar titanoclinohumite defects (Kitamura et al. 1987; Mosenfelder et al. 2004).

The **E**∥a spectra in our hydrothermally grown olivines are dominated by the same high-wavenumber bands seen in the study of Kohlstedt et al. (1996), in which H diffused into relatively large crystals of San Carlos olivine. Different starting olivines yielded spectra with nearly identical band structure (Fig. 4), despite the difference in initial speciation (i.e., the bands attributed to humite in Zabargad olivine). The strongest bands are at 3613, 3598, 3579, and 3567 cm^{-1}, and the heights of the peaks increase with increasing water fugacity (Fig. 5). Note that the height of the most intense peaks may be underestimated in some samples, because the extinction ratio of the polarizer becomes increasingly important as the absorbance approaches a high value (close to 2) (Libowitzky and Rossman 1996). This could explain, for instance, the apparent change in relative peak intensities near 3613 and 3598 cm^{-1} as water fugacity increases (Fig. 5). However, this should have a minimal effect on the integrated absorbance over the entire OH-stretching range.

In addition to the strong bands discussed above, most spectra in the present study show a triplet of absorption bands at 3502, 3483, and 3456 cm^{-1}. These bands, also observed in the Buell Park olivine shown in Figure 3, are prominently observed only in one unpolarized spectrum (at 12 GPa, 1100 °C) presented by

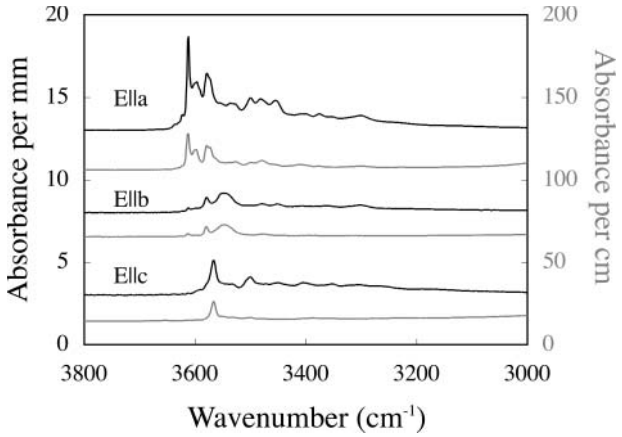

Figure 3. Polarized IR spectra from an experimental sample (ww227, 8 GPa, 1150 °C, 24 h) and a natural crystal of olivine from the Buell Park diatreme in Arizona (no. GRR1629). Experimental (black) and natural (gray) sample spectra are normalized to 1 mm and 1 cm absorbance, respectively, and offset arbitrarily for the sake of comparison. The spectra for ww227 are synthesized using the technique outlined in the text, and are baseline corrected. The spectra from the Buell Park sample were acquired on an oriented single crystal, and are not corrected for baseline. The **E**-vector of each spectrum is noted in the figure.

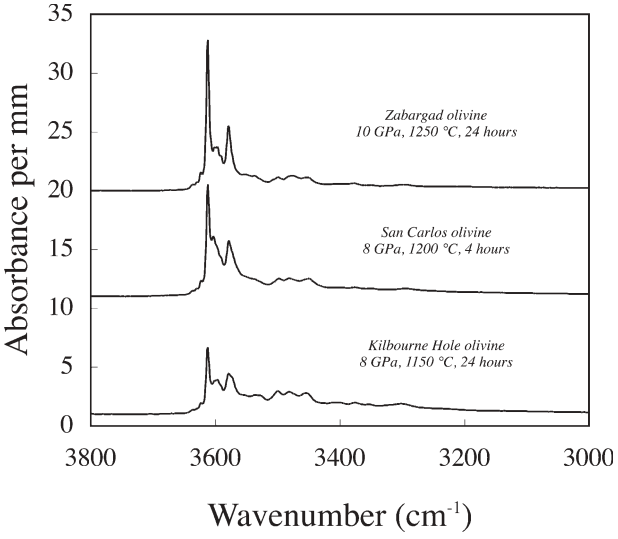

Figure 4. Synthetic **E**∥a IR spectra for olivine from three different experiments that used three different starting materials. The starting olivine material and conditions of the experiments are annotated in the figure. The run numbers (see Table 1), starting from the top of the figure going down, are ww256, ww325, and ww227.

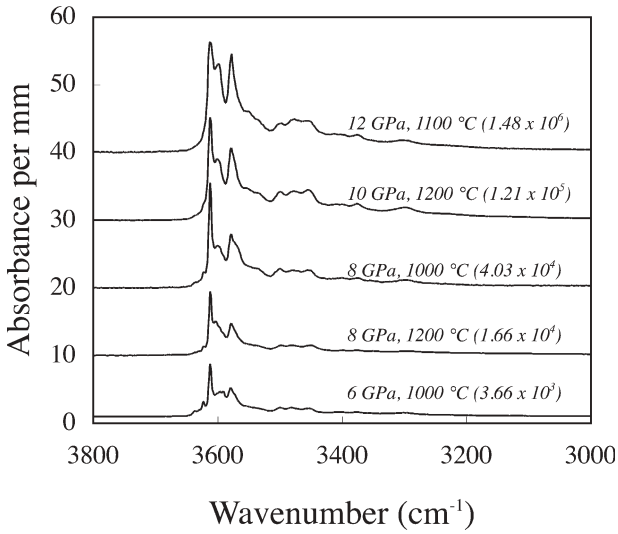

Figure 5. **E**∥a IR spectra (synthetic) for olivine from five experiments, showing the increase in absorption with increasing water fugacity. The conditions and water fugacity (in parentheses) for each experiment are annotated in the figure. Water fugacity was calculated according to the equation of state for water of Pitzer and Sterner (1994), as discussed in the text. The peak height for the 3613 cm^{-1} band in the uppermost spectrum may be underestimated, as discussed in the text.

Kohlstedt et al. (1996), and were not observed in lower pressure studies (Bai and Kohlstedt 1993; Zhao et al. 2004). Olivine in the latter studies also exhibits prominent bands at 3525 and 3573 cm^{-1} that are not observed in this study. These differences may reflect fundamental changes in the incorporation mechanism of hydrogen in olivine between low pressure (<1 GPa) and high-pressure experimental studies.

Another notable feature of the spectra in this study is the low intensity or complete lack of strong absorption bands in the region between 3300 and 3400 cm^{-1}. These bands were generally seen in samples annealed at higher oxygen fugacities in the study of Bai and Kohlstedt (1993). Matveev et al. (2001, 2005) also observed these bands in samples annealed in the presence of orthopyroxene, and attributed them to high silica activity rather than to high oxygen fugacity.

Measured OH concentrations in the present study are given in Table 1, and compared to the measurements of Bai and Kohlstedt (1993) and Kohlstedt et al. (1996) in a log-log plot of concentration against water fugacity in Figure 6. The water fugacity was calculated using the equation of state for water of Pitzer and Sterner (1994). Our values for water fugacity differ by about 13–14% from those calculated by Kohlstedt et al. (1996), and we have replotted their data with our recalculated values; the conclusions of our study are not dependent on this discrepancy, however. The results show a difference of 2.5 to 4 in absolute values between our study and that of Kohlstedt et al. (1996).

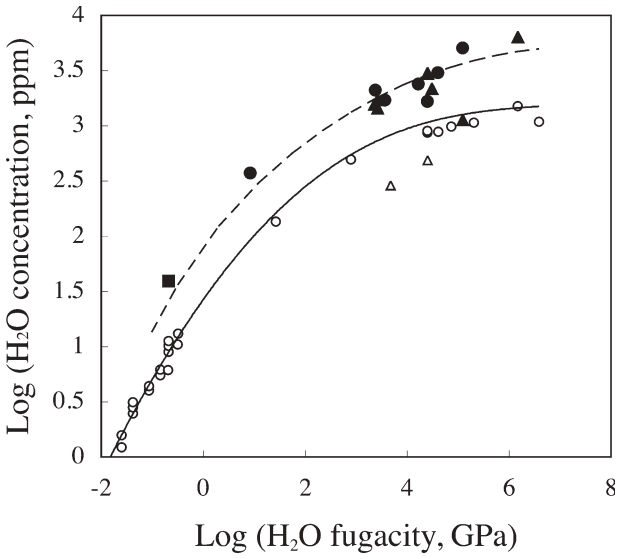

FIGURE 6. Log-log plot of OH concentration in olivine (expressed as ppm H_2O) vs. water fugacity. The open circles are previous data from Bai and Kohlstedt (1993) and Kohlstedt et al. (1996), for experiments in which excess H_2O was present after the experiment. Open triangles are experiments from Kohlstedt et al. (1996) for which there was no excess water. The filled square is a re-estimation by Bell et al. (2003) of the OH concentration for an experiment from Bai and Kohlstedt (1993). The filled circles and triangles represent experiments from the present study for which excess water was present or absent, respectively, after the experiment. The lines are calculated using the equation given in the text. The solid line is calculated using the parameters given by Kohlstedt et al. (1996), and the dashed line is calculated using the new parameters derived only from our experiments where excess water was present.

Hydrogen incorporation in Fo_{100}

Results of the two experiments we performed in the nominally pure MgO-SiO_2-H_2O system were surprisingly different, despite a similarity in *P-T* conditions. In experiment ww276 at 5.65 GPa, the temperature was first held above the solidus (Inoue 1994) at 1300 °C for 15 h. Subsequently, the temperature was decreased at a rate of 50 °C/min to 1175 °C and held for 15 h. The end product (Fig. 2d) consisted of forsterite crystals with diameters up to ~500 μm, with a small amount of fine-grained (5–10 μm) crystals of MgO concentrated on the bottom of the capsule. Measured FeO concentrations were below the detection limit of 0.02 wt% (Table 2). IR spectra (Fig. 7a) reveal the

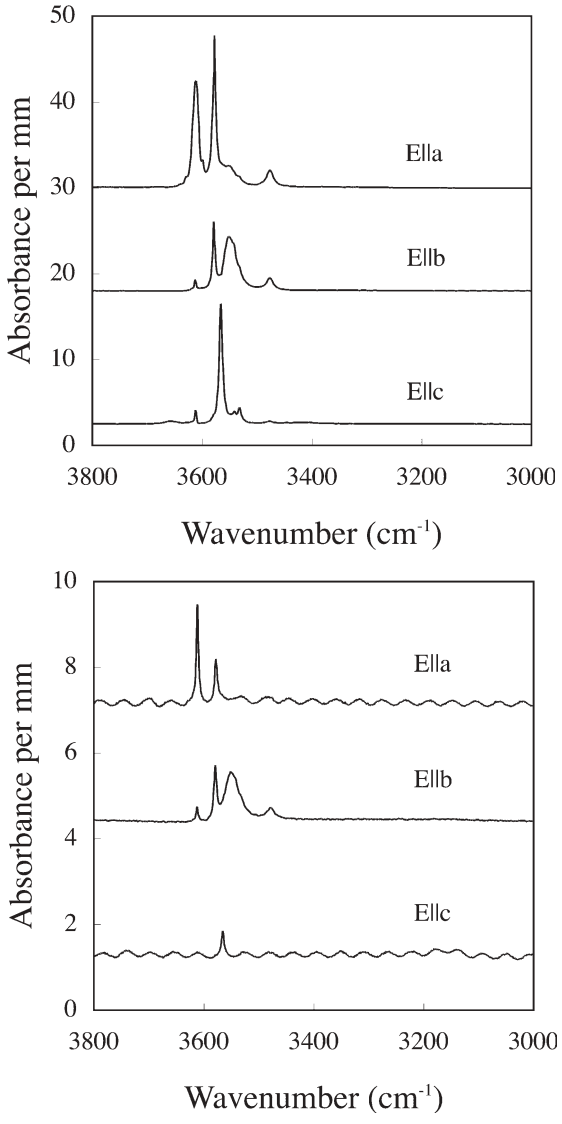

FIGURE 7. Polarized IR spectra from Mg_2SiO_4 forsterite crystals in two experiments. All spectra are normalized to 1 mm and baseline corrected. (**a**) Synthetic polarized IR spectra for forsterite from ww276, crystallized from a partial melt at 5.65 GPa (see Fig. 2d). (**b**) Polarized IR spectra collected from two single crystals recovered in experiment ww331 from 6 GPa, 1200 °C. The sinusoidal interference fringes are caused by reflection of light off the polished surfaces of the crystal. The **E**-vector of each spectrum is noted in the figure.

same features as in the experiments of Lemaire et al. (2004) at low silica activity. The concentration of OH in these olivines is comparable to that of Fo_{90} at similar conditions (Table 1).

In contrast, in experiment ww331, conducted at 6 GPa using oriented single crystals, OH concentrations were much lower (Fig. 7b). Polarized IR spectra of these crystals are similar to those of forsterite in the studies of Demouchy and Mackwell (2003) and Zhao et al. (2004). The duration of this experiment was chosen so as to limit water loss from the sample, while ensuring homogenization of OH according to the diffusion data of Demouchy and Mackwell (2003). Nevertheless, distinct zoning profiles of OH were observed in the sample. The spectra shown in Figure 7b represent the highest absorption measured in the samples. The large difference in OH concentrations between the two Fo_{100} experiments is discussed below.

DISCUSSION

Mechanisms of hydrogen incorporation

In the following discussion, we refer to three groups of absorption bands in olivine. Following Bai and Kohlstedt (1993), Group I bands occur in the range 3450–3650 cm^{-1}, and Group II bands are in the range 3200–3450 cm^{-1}. We also distinguish a subset of Group I, hereafter referred to as "Group I-H," represented by strong bands at 3525 and 3573 cm^{-1}. All of these bands are strongly anisotropic, with the greatest absorption along **E**||a.

Many hypotheses have been put forward to explain the incorporation of hydrogen in olivine. Point defects have been linked to hydrogen incorporation, but the question of which point defect predominates under what conditions is controversial, and it is not possible to obtain unique assignments for olivine based on dipole directions and the wavenumber dependence of IR bands (e.g., Lemaire et al. 2004). Despite attempts to correlate trace element concentrations in olivine with H content (e.g., Kurosawa et al. 1997), boron is the only element clearly demonstrated to play a role in hydrogen incorporation via coupled substitution (Kent and Rossman 2002), and is unlikely to play an important role at high OH concentrations. Studies of natural olivines using spectroscopy and electron microscopy have demonstrated that OH can be incorporated into olivine via nm- to μm-scale inclusions or planar defects of hydrous phases, including talc, serpentine, and various humite-series minerals (Kitamura et al. 1987; Miller et al. 1987; Khisina et al. 2001; Matsyuk and Langer 2004; Mosenfelder et al. 2004). A structure of "hydrous modified olivine" has also been proposed based on electron microscopy (Khisina et al. 2001) and modeling (Kudoh 2002). This defect locally has the structure of clinohumite, and can also be considered as an ordered array of point defects.

The hydrous phases that may be included in olivine exhibit distinct IR bands (Miller et al. 1987; Matsyuk and Langer 2004). None of the bands corresponding to talc or serpentine are observed in our experimentally hydrated olivines. Group I-H bands, which are common in the majority of natural, H-bearing olivines, were attributed to humite by Miller et al. (1987), and may also represent a humite-related defect that is not detectable optically (for instance, the hydrous modified olivine structure proposed by Kudoh 2002). We also do not observe these bands in our experimental study, but note that they are the dominant bands in lower-pressure experiments (Bai and Kohlstedt 1993; Zhao et al. 2004). Berry et al. (2004) also produced olivines with these bands, and attributed them to the presence of Ti. Trace amounts of Ti may stabilize a defect related to titanoclinohumite, which exhibits Type I-H bands as well as a prominent band near 3400 cm^{-1} (Kitamura et al. 1987), which is apparently missing in the experimental studies.

We conclude that incorporation of hydrogen via inclusions of hydrous phases is unlikely to be an important mechanism in our experiments or those of Kohlstedt et al. (1996), although electron microscopy is needed to verify this hypothesis. This may reflect a change in incorporation mechanism between olivines hydrated at low pressures, where "hydrous modified olivine" or another humite-related defect dominates, and high pressures, where disordered point defects dominate. Ancillary evidence for this hypothesis comes from the close correspondence in band positions between our samples and the natural olivine from Buell Park (Fig. 3); the exact *P-T* conditions of formation for this xenocryst are unknown, but derivation from conditions in the garnet peridotite stability field is likely based on association with pyropic garnets and chromian diopside (Smith and Levy 1976).

Bai and Kohlstedt (1993) and Kohlstedt et al. (1996) promoted incorporation via oxygen interstitials (balanced by two protons), but this idea was later dropped in favor of metal vacancies (Kohlstedt and Mackwell 1998). Brodholt and Refson (2000) delineated a more important role for Si vacancies on the basis of ab initio calculations showing that the concentration of Si vacancies is enhanced relative to metal vacancies under wet conditions. More recently, Matveev et al. (2001, 2005) argued that silica activity plays a crucial, previously unrecognized role, resulting in fundamentally different IR band structures at different conditions. They ascribed Group I bands to Si vacancies formed under conditions of low silica activity, and Group II bands to metal vacancies formed at higher silica activity in equilibrium with orthopyroxene. A surprising conclusion of their study is that olivines from orthopyroxene-bearing peridotite sources (Miller et al. 1987) are suggested to have been re-equilibrated at lower silica activity (based on the predominance of Group I bands). Their experimental results contradict those of Bai and Kohlstedt (1993), who showed no evidence for a significant effect of silica activity on incorporation mechanism. Matveev et al. (2001) also suggested that the olivines in experiments by Bai and Kohlstedt (1993) and Kohlstedt et al. (1996) were not in equilibrium because of an apparent lack of Fe-Mg exchange between the olivine and the silica buffer.

One aspect of the experiments by Matveev et al. (2001) that has not been discussed is that they were conducted at higher oxygen fugacity (buffered at Re-ReO_2; see Pownceby and O'Neill 1994) than the experiments of Kohlstedt et al. (1996), which were buffered at Ni-NiO. Bai and Kohlstedt (1993) also conducted high-pressure experiments using olivines pre-equilibrated over a wide range of oxygen fugacities at 1 atm, and demonstrated that the intensity of the Group II bands increased with increasing pre-annealing oxygen fugacity. More recently, Zhao et al. (2004) demonstrated a trend of increasing intensity of Group II bands with increasing temperature, which could also be related to increasing oxygen fugacity (either increasing with temperature, or increasing due to exhaustion of the buffer).

Lemaire et al. (2004) also examined the effect of varying silica activity on hydrogen incorporation, in nominally pure

Mg_2SiO_4 olivine. They demonstrated that, with increasing silica activity, the intensity of Group I bands decreases, but that the bands do not disappear, in contrast with the results of Matveev et al. (2001). The Group II bands seen in Fe-bearing samples were not observed, but two additional bands were seen at even lower wavenumbers, at 3160 and 3220 cm^{-1}. These bands exhibit a broader FWHM than other bands, and also exhibit distinctly different anisotropy, appearing in **E**||c spectra only. The band at 3160 cm^{-1} has not been seen in natural olivines, to our knowledge, but the band at 3220 cm^{-1} nearly corresponds to a band seen in Zabargad olivine, with the same anisotropy (Beran and Putnis 1983). This band was attributed by Lemaire et al. (2004) to metal vacancies at high silica activity. However, it can also be attributed to a humite-type defect, as it is seen in the spectra of humite-type minerals (Matsyuk and Langer 2004).

In our experiments, which were nominally either buffered at high silica activity (in the presence of orthopyroxene) or unbuffered, we only see Group I bands. We therefore suggest that the band assignments of Matveev et al. (2001) are either incorrect or that there is a fundamental change in incorporation mechanism under high silica activity conditions between their experiments, at pressures of 2 GPa and below, and those at higher pressures (this study and Kohlstedt et al. 1996).

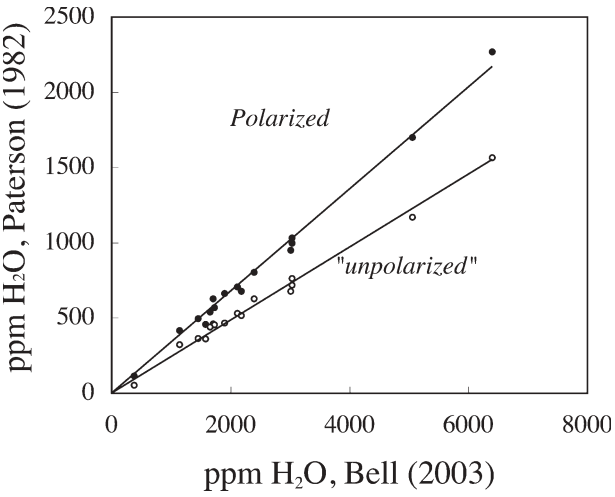

FIGURE 8. Comparison among IR calibrations applied to our experimental samples. Filled and unfilled circles are for polarized and unpolarized IR spectra, respectively. Spectra were calculated as discussed in the text. Regression lines constrained to pass through the origin indicate that the Bell et al. (2003) calibration gives 2.95 or 4.12 times the amount of the Paterson (1982) calibration for polarized and unpolarized radiation, respectively.

Calibration of OH in olivine

Bell et al. (2003) showed that their new calibration for OH in olivine differed systematically from that of Paterson (1982) by a factor of either 2.3 or 3.5, depending on whether the analysis was carried out using polarized or unpolarized IR spectra, respectively. They reiterated the warning of Libowitzky and Rossman (1996) that the use of unpolarized radiation can introduce non-systematic errors into the analysis, due to partial polarization of the beam absorption intensities, which are not a linear function of thickness. Nevertheless, several authors have adopted the 3.5 correction factor (Koga et al. 2003; Aubaud et al. 2004; Bolfan-Casanova 2005; Katayama et al. 2005).

In Figure 8, we show a comparison for our samples indicating that OH concentrations derived using the Bell et al. (2003) calibration are, on average, 2.95 and 4.12 times the amount calculated using the Paterson (1982) calibration for polarized and unpolarized radiation, respectively. This disparity with Bell et al. (2003) may reflect differences in the spectra of olivines with much larger OH concentrations than those analyzed by Bell et al. (2003); in other words a larger proportion of integrated area at lower wavenumbers may skew the wavenumber-dependent Paterson (1982) analysis. Alternatively, the Bell et al. (2003) calibration may not extrapolate linearly to higher OH concentrations. This possibility remains to be solved using alternate calibration methods. In any case, we reiterate that the use of "unpolarized" radiation in IR studies is subject to non-systematic errors and that correction of the data of Kohlstedt et al. (1996) and Zhao et al. (2004) is not straightforward.

Thermodynamics of OH solubility

The thermodynamics of OH solubility in olivine have been discussed extensively elsewhere. Kohlstedt et al. (1996) modeled the dependence of OH solubility on pressure up to 13 GPa, whereas Zhao et al. (2004) investigated the effects of temperature and Fe content at low pressure. It is important to note, as discussed above, that the mechanism of hydrogen incorporation in olivine in the low-pressure experiments may be fundamentally different from that in high-pressure experiments. Therefore, derivation of a global set of parameters from these two studies (Bercovici and Karato 2003) may not be strictly valid.

Unfortunately, the OH concentrations of olivines in the present study exhibit too much scatter to derive a meaningful function of OH solubility with temperature or Fe-content at high pressure. Therefore, we restrict ourselves to an analysis similar to that of Kohlstedt et al. (1996), using their Equation 16:

$$C_{OH} = A f_{H_2O}^{n} \exp(-P\Delta V / RT)$$

where C_{OH} is the concentration of OH in olivine expressed as H/10^6 Si, A is a constant, f_{H_2O} is the fugacity of water, ΔV is the change in molar volume of the olivine lattice due to hydrogen incorporation, R is the gas constant, and P and T are pressure and temperature. The exponent n for water fugacity is 1 whether the mechanism of incorporation involves two hydrogen atoms substituted in a metal vacancy or bonded to an oxygen interstitial (see Kohlstedt et al. 1996). For simplicity we assume T = 1373 K even though our experiments vary in temperature from 1273 to 1573 K. We fit the equation only to experiments in which excess water was present (Table 1). The analysis yields A = 2.45 H/10^6 Si/GPa and $\Delta V = 10.2 \times 10^{-6}$ m^3/mol. The value for ΔV is thus indistinguishable from the values of 10.6×10^{-6} m^3/mol and 10.0×10^{-6} m^3/mol calculated by Kohlstedt et al. (1996) and Zhao et al. (2004), respectively. The fit to all the data with these parameters is shown in Figure 6 as a dashed line. The new values indicate an OH solubility 2.2–3.4 times higher than that of Kohlstedt et al. (1996). Clearly, more work is needed to accurately assess the effects of temperature, Fe content, silica

activity and oxygen fugacity at the high pressures (up to 13 GPa) relevant to the entire upper mantle.

Attainment of equilibrium in studies of hydrogen incorporation

The question of whether hydrogen incorporation experiments have reached equilibrium has rarely been addressed (cf. Bromiley et al. 2004). In our experiments on Fe-bearing olivine, we are encouraged by the fact that the IR spectra of the products are similar regardless of starting material or mode of incorporation (i.e., during grain growth vs. via diffusion into larger crystals), and that the crystals do not exhibit zoning profiles in OH concentration. The discrepancy in OH concentrations in our two experiments on Mg_2SiO_4 forsterite is disturbing, however. There is no obvious difference in composition of the two starting materials that could account for this discrepancy.

The inferred solubility of OH in Mg_2SiO_4 forsterite varies by orders of magnitude in the literature, from very low values (Keppler and Rauch 2000; Demouchy et al. 2003; Zhao et al. 2004) to values equal to or higher than that for Fe-bearing olivine at comparable conditions (Kohn 1996; Locke et al. 2001; Lemaire et al. 2004). This discrepancy can even be observed within a single study. Lemaire et al. (2004) produced forsterites with either 60 or 750 ppm H_2O in two separate experiments, even though both runs were saturated with H_2O, and the composition, pressure, temperature and cooling rate from above the liquidus were all nominally identical. Lemaire et al. (2004) inferred that cooling rate was an important factor in OH solubility, but the details of this relationship are not well constrained. We are left with the troubling conclusion that disequilibrium effects may attend hydrogen incorporation during growth of crystals from a melt or partial melt, and inferring OH solubility from such experiments is dangerous. Kinetic effects may also play a complex role in incorporation of OH by diffusion into large crystals, even when diffusion rates are nominally constrained (Bromiley et al. 2004).

Geophysical and geochemical implications

Our new results indicate that models need to be revised for processes that are affected by a high solubility of OH in olivine, such as partitioning of hydrogen between olivine and other phases during melting (Hirth and Kohlstedt 1996; Asimow and Langmuir 2003), and viscosity of hydrous zones in the mantle (Hirth and Kohlstedt 1996; Dixon et al. 2004). Although the change in estimated bulk partition coefficient for H_2O between melt and fertile peridotite due to our revised estimate of OH solubility is small (about 30%), the difference would increase during partial melting as the modal abundance of olivine in the residue increases. On a broader scale, Bercovici and Karato (2003) recently presented an intriguing model that attempts to reconcile geochemical and geophysical constraints on mantle convection. One of the postulates of their "transition zone water filter" hypothesis is that a sharp contrast in OH solubility between minerals of the transition zone (with high solubility represented by wadsleyite) and the upper mantle (represented by olivine) can result in the formation of hydrous melts at the 410 km discontinuity that sequester trace elements. They also propose that hot mantle plumes can "bypass" this filter because the solubility in olivine increases with temperature while that of wadsleyite decreases with temperature. These legs of the hypothesis hinge on experimental constraints on OH solubility such as those presented here.

Our updated estimate for OH solubility in olivine reduces the contrast in solubility inferred by Bercovici and Karato (2003), because estimates of hydrogen solubility in wadsleyite are based on different methods that remain robust at high hydrogen content: SIMS analyses (Demouchy et al. 2005) and X-ray diffraction (Smyth 1994). This conclusion was also reached by Hirschmann et al. (2005), on the basis of SIMS measurements and the work of Bell et al. (2003). The simple thermodynamic model of Bercovici and Karato (2003) for the dependence of OH solubility on pressure and temperature hinges on an extreme extrapolation of the low-pressure data (Zhao et al. 2004), which may be complicated by changes in incorporation mechanism between low- and high-pressure experiments as discussed above. Furthermore, Hirschmann et al. (2005) speculated that changes in fluid chemistry at high pressures might reverse the temperature dependence of OH solubility in olivine. Bercovici and Karato (2003) also ignored the contribution of pyroxenes to the water storage capacity of the upper mantle. Finally, the inference that OH solubility in wadsleyite and ringwoodite decreases with temperature was based at the time on only a few experiments, many of which were conducted at water-undersaturated conditions in the presence of a melt (Ohtani et al. 2000). Although subsequent experiments have borne out this trend (Demouchy et al. 2005), they demonstrate that the decrease in OH content of wadsleyite above 1200 °C results from decreasing H_2O activity in the coexisting fluid as it becomes, either continuously or discontinuously, more melt-like. Extrapolation of these results to Fe-bearing compositions is highly uncertain. Clearly, more mineral physics constraints are needed to evaluate the transition zone water filter hypothesis.

Acknowledgments

Financial support for this investigation was provided by NSF grants OCE-0095294 and OCE-0241716 to P.D.A. and EAR-0337816 to G.R.R. We thank Shun Karato for donation of the synthetic forsterite crystal and Mike Baker for donation of olivines and pyroxenes from Kilbourne Hole. Bruce Watson gave expert advice and encouragement on encapsulation techniques. Chi Ma and Elizabeth Miura are thanked for their assistance with electron microprobe and infrared analyses, respectively. Finally, we thank Eugen Libowitzky, Hans Keppler, and an anonymous referee for constructive reviews that improved the manuscript.

References cited

Armstrong, J.T. (1988) Quantitative analysis of silicate and oxide minerals, comparison of Monte Carlo, ZAF and φ(ρz) procedures. In D.E. Newbury, Ed., Microbeam analysis, p. 239–246. San Francisco Press, California.

Arredondo, E.H. and Rossman, G.R. (2002) Feasibility of determining the quantitative OH content of garnets with Raman spectroscopy. American Mineralogist, 87, 307–311.

Asimow, P.D. and Langmuir, C.H. (2003) The importance of water to oceanic mantle melting regimes. Nature, 421, 815–820.

Asimow, P.D., Stein, L.C., Mosenfelder, J.L., and Rossman, G.R. (2006) Quantitative polarized FTIR analysis of trace OH in populations of randomly oriented mineral grains. American Mineralogist, 91, 278–284.

Aubaud, C., Hauri, E., and Hirschmann, M.M. (2004) Hydrogen partition coefficients between nominally anhydrous minerals and basaltic melts. Geophysical Research Letters, 31, DOI: 10.1029/2004GL021341.

Ayers, J.C., Brenan, J.B., Watson, E.B., Wark, D.A., and Minarik, W.G. (1992) A new capsule technique for hydrothermal experiments using the piston-cylinder apparatus. American Mineralogist, 77, 1080–1086.

Bai, Q. and Kohlstedt, D.L. (1993) Effects of chemical environment on the solubility and incorporation mechanism for hydrogen in olivine. Physics and Chemistry of Minerals, 19, 460–471.

Bell, D.R., Rossman, G.R., Maldener, J., Endisch, D., and Rauch, F. (2003) Hydroxide in olivine: a quantitative determination of the absolute amount and

calibration of the IR spectrum. Journal of Geophysical Research, 108(2105), 10.1029/2001JB000679.
Beran, A. and Putnis, A. (1983) A model of the OH positions in olivine, derived from infrared-spectroscopic investigations. Physics and Chemistry of Minerals, 9, 57–60.
Bercovici, D. and Karato, S.-I. (2003) Whole-mantle convection and the transition-zone water filter. Nature, 425, 39–44.
Berry, A., Hermann, J., and O'Neill, H. (2004) The water site in mantle olivine. Geochimica et Cosmochimica Acta, 68, A36.
Bohlen, S.R. and Boettcher, A.L. (1982) The quartz-coesite transformation: a precise determination and the effects of other components. Journal of Geophysical Research, 87(B8), 7073–7078.
Bolfan-Casanova, N. (2005) Water in the Earth's mantle. Mineralogical Magazine, 69, 229–257.
Bolfan-Casanova, N., Keppler, H., and Rubie, D.C. (2000) Water partitioning between nominally anhydrous minerals in the MgO-SiO_2-H_2O system up to 24 GPa: implications for the distribution of water in the Earth's mantle. Earth and Planetary Science Letters, 182, 209–221.
Brodholt, J.P. and Refson, K. (2000) An ab initio study of hydrogen in forsterite and a possible mechanism for hydrolytic weakening. Journal of Geophysical Research, 105, 18,977–18,982.
Bromiley, G.D., Keppler, H., McCammon, C., Bromiley, F.A., and Jacobsen, S.D. (2004) Hydrogen solubility and speciation in natural, gem-quality chromian diopside. American Mineralogist, 89, 941–949.
Demouchy, S. and Mackwell, S. (2003) Water diffusion in synthetic iron-free forsterite. Physics and Chemistry of Minerals, 30, 486–494.
Demouchy, S., Deloule, E., Frost, D.J., and Keppler, H. (2005) Pressure and temperature-dependence of water solubility in Fe-free wadsleyite. American Mineralogist, 90, 1084–1091.
Dixon, J.E., Dixon, T.H., Bell, D.R., and Malservisi, R. (2004) Lateral variation in upper mantle viscosity: role of water. Earth and Planetary Science Letters, 222, 451–467.
Frost, D.J., Poe, B.T., Trønnes, R.G., Liebske, C., Duba, A., and Rubie, D.C. (2004) A new large-volume multianvil system. Physics of the Earth and Planetary Interiors, 143–144, 507–514.
Getting, I.C. (1998) New determination of the bismuth I-II equilibrium pressure: a proposed modification to the practical pressure scale. Metrologia, 35, 119–132.
Hirschmann, M.M., Aubaud, C., and Withers, A.C. (2005) Storage capacity of H_2O in nominally anhydrous minerals in the upper mantle. Earth and Planetary Science Letters, 236, 167–181.
Hirth, G. and Kohlstedt, D.L. (1996) Water in the oceanic upper mantle: implications for rheology, melt extraction and the evolution of the lithosphere. Earth and Planetary Science Letters, 144, 93–108.
Holland, T.J.B. (1980) The reaction albite = jadeite + quartz determined experimentally in the range 600–1200 °C. American Mineralogist, 65, 129–134.
Inoue, T. (1994) Effect of water on melting phase relations and melt composition in the system Mg_2SiO_4-$MgSiO_3$-H_2O up to 15 GPa. Physics of the Earth and Planetary Interiors, 85, 237–263.
Karato, S.-I. (1989) Grain growth kinetics in olivine aggregates. Tectonophysics, 168, 255–273.
Karato, S.-I. (2003) Mapping water content in the upper mantle: rheological and seismic consequences. In J. Eiler, Ed., Inside the Subduction Factory. American Geophysical Union, Washington, D.C.
Katayama, I., Karato, S.-I., and Brandon, M. (2005) Evidence of high water content in the deep upper mantle inferred from deformation microstructures. Geology, 33, 613–616.
Kent, A.J.R. and Rossman, G.R. (2002) Hydrogen, lithium, and boron in mantle-derived olivine: the role of couple substitutions. American Mineralogist, 87, 1432–1436.
Keppler, H. and Rauch, M. (2000) Water solubility in nominally anhydrous minerals measured by FTIR and ^{1}H MAS NMR: the effect of sample preparation. Physics and Chemistry of Minerals, 27, 371–376.
Khisina, N.R. and Wirth, R. (2002) Hydrous olivine $(Mg_{1-y}Fe^{2+}_y)_{2-x}v_xSiO_4H_{2x}$—a new DHMS phase of variable composition observed as nanometer-sized precipitations in mantle olivine. Physics and Chemistry of Minerals, 29, 98–111.
Khisina, N.R., Wirth, R., Andrut, M., and Ukhanov, A.V. (2001) Extrinsic and intrinsic mode of hydrogen occurrence in natural olivines: FTIR and TEM investigation. Physics and Chemistry of Minerals, 28, 291–301.
Kitamura, M., Kondoh, S., Morimoto, N., Miller, G.H., Rossman, G.R., and Putnis, A. (1987) Planar OH-bearing defects in mantle olivine. Nature, 328, 143–145.
Koga, K., Hauri, E., Hirschmann, M., and Bell, D. (2003) Hydrogen concentration analyses using SIMS and FTIR: comparison and calibration for nominally anhydrous minerals. Geochemistry, Geophysics, and Geosystems, 4, DOI: 10.1029/2002GC000378.
Kohlstedt, D.L. and Mackwell, S.J. (1998) Diffusion of hydrogen and point defects in olivine. Zeitschrift für Physikalische Chemie, 207, 147–162.
Kohlstedt, D.L., Keppler, H., and Rubie, D.C. (1996) Solubility of water in the α, β, and γ phases of $(Mg, Fe)_2SiO_4$. Contributions to Mineralogy and Petrology, 123, 345–357.
Kohn, S.C. (1996) Solubility of H_2O in nominally anhydrous mantle minerals using ^{1}H MAS NMR. American Mineralogist, 81, 1523–1526.
Kudoh, Y. (2002) Predicted model for hydrous modified olivine (HyM-α). Physics and Chemistry of Minerals, 29, 387–395.
Kurosawa, M., Yurimoto, H., and Sueno, S. (1997) Patterns in the hydrogen and trace element compositions of mantle olivines. Physics and Chemistry of Minerals, 24, 385–395.
Lemaire, C., Kohn, S.C., and Brooker, R.A. (2004) The effect of silica activity on the incorporation mechanisms of water in synthetic forsterite: a polarised infrared spectroscopic study. Contributions to Mineralogy and Petrology, 147, 48–57.
Libowitzky, E. and Rossman, G.R. (1996) Principles of quantitative absorption measurements in anisotropic crystals. Physics and Chemistry of Minerals, 23, 319–327.
Locke, D.R., Holloway, J.R., Leinenweber, K., and Hervig, R. (2001) Effect of MgO/SiO_2 activity ratio on H_2O solubility in forsterite. EOS Transactions AGU, 82 (47), Abstract T21B-0890.
Martin, R.F. and Donnay, G. (1972) Hydroxyl in the mantle. American Mineralogist, 57, 554–570.
Matsyuk, S.S. and Langer, K. (2004) Hydroxyl in olivines from mantle xenoliths in kimberlites from the Siberian platform. Contributions to Mineralogy and Petrology, 147, 413–437.
Matveev, S., O'Neill, H.S.C., Ballhaus, C., Taylor, W.R., and Green, D.H. (2001) Effect of silica activity on OH-IR spectra of olivine: implications for low-$a$$SiO_2$ mantle metasomatism. Journal of Petrology, 42, 721–729.
Matveev, S., Portnyagin, M., Ballhaus, C., Brooker, R., and Geiger, C.A. (2005) FTIR spectrum of phenocryst olivine as an indicator of silica saturation in magmas. Journal of Petrology, 46, 603–614.
Miller, G.H., Rossman, G.R., and Harlow, G.E. (1987) The natural occurrence of hydroxide in olivine. Physics and Chemistry of Minerals, 14, 461–472.
Morishima, H., Kato, T., Suto, M., Ohtani, E., Urakawa, S., Utsumi, W., Shimomura, O., and Kikegawa, T. (1994) The phase boundary between α-and β-Mg_2SiO_4 determined by in situ X-ray diffraction. Science, 265, 1202–1203.
Mosenfelder, J.L., Sharp, T.G., Asimow, P.D., and Rossman, G.R. (2004) Hydrogen in olivines from the Colorado Plateau: implications for water in the mantle and the Alpe Arami controversy. EOS Trans AGU, 85(47), Abstract T32B-07.
Ohtani, E., Mizobata, H., and Yurimoto, H. (2000) Stability of dense hydrous magnesium silicate phases in the systems Mg_2SiO_4-H_2O and $MgSiO_3$-H_2O at pressures up to 27 GPa. Physics and Chemistry of Minerals, 27, 533–544.
Paterson, M.S. (1982) The determination of hydroxyl by infrared-absorption in quartz, silicate-glasses and similar materials. Bulletin de Mineralogie, 105, 20–29.
Pitzer, K.S. and Sterner, S.M. (1994) Equations of state valid continuously from zero to extreme pressures for H_2O and CO_2. Journal of Chemical Physics, 101, 3111–3116.
Pownceby, M.I. and O'Neill, H.S.C. (1994) Thermodynamic data from redox reactions at high temperatures. IV. Calibration of the Re-ReO_2 oxygen buffer from EMF and NiO + Ni-Pd redox sensor measurements. Contributions to Mineralogy and Petrology, 118, 130–137.
Rubie, D.C. (1999) Characterising the sample environment in multianvil high-pressure experiments. Phase Transitions, 68, 431–451.
Smith, D. and Levy, S. (1976) Petrology of the Green Knobs diatreme and implications for the upper mantle below the Colorado Plateau. Earth and Planetary Science Letters, 29, 107–125.
Smyth, J.R. (1994) A crystallographic model for hydrous wadsleyite (β-Mg_2SiO_4): an ocean in the Earth's interior. American Mineralogist, 79, 1021–1024.
Susaki, J., Akaogi, M., Akimoto, S., and Shimomura, O. (1985) Garnet-perovskite transformation in $CaGeO_3$: in situ X-ray measurements using synchrotron radiation. Geophysical Research Letters, 12, 729–732.
Takei, H. and Kobayashi, T. (1974) Growth and properties of Mg_2SiO_4 single crystals. Journal of Crystal Growth, 23, 121–124.
Tarits, P., Hautot, S., and Perrier, F. (2004) Water in the mantle: results from electrical conductivity beneath the French Alps. Geophysical Research Letters, 31, L06612, 10.1029/2003GL019277.
Truckenbrodt, J. and Johannes, W. (1999) H_2O loss during piston-cylinder experiments. American Mineralogist, 84, 1333–1335.
Wasylenki, L.E., Baker, M.B., Kent, A.J.R., and Stolper, E.M. (2003) Near-solidus melting of the shallow upper mantle: partial melting experiments on depleted peridotite. Journal of Petrology, 44, 1163–1191.
Watson, E.B. and Cherniak, D.J. (1997) Oxygen diffusion in zircon. Earth and Planetary Science Letters, 148, 527–544.
Zhang, J., Li, B., Utsumi, W., and Liebermann, R.C. (1996) In situ X-ray observations of the coesite-stishovite transition: reversed phase boundary and kinetics. Physics and Chemistry of Minerals, 23, 1–10.
Zhao, Y.-H., Ginsberg, S.B., and Kohlstedt, D.L. (2004) Solubility of hydrogen in olivine: dependence on temperature and iron content. Contributions to Mineralogy and Petrology, 147, 155–161.

MANUSCRIPT RECEIVED MARCH 11, 2005
MANUSCRIPT ACCEPTED SEPTEMBER 20, 2005
MANUSCRIPT HANDLED BY GEORGE LAGER